# Oscillatory instability in a reaction front separating fluids of different densities

Dan Coroian[1] and Desiderio A. Vasquez[2,3]
[1]*Department of Mathematical Sciences, Purdue University Fort Wayne, Fort Wayne, Indiana 46805, USA*
[2]*Department of Physics, Purdue University Fort Wayne, Fort Wayne, Indiana 46805, USA*
[3]*Departamento de Ciencias, Sección Física, Pontificia Universidad Católica del Perú, Av. Universitaria 1801, San Miguel, Lima 32, Peru*

(Received 24 April 2018; published 6 August 2018)

Reaction fronts described by the Kuramoto-Sivashinsky (KS) equation can exhibit complex behavior as they separate reacted from unreacted fluids. If the fluid of higher density is above a fluid of lower density, then the Rayleigh-Taylor instability can lead to fluid motion. In the reverse situation, where the lighter fluid is on top, gravitationally driven forces can stabilize a convectionless flat front inhibiting the complex front propagation described by the KS equation. In these cases, a critical density difference is required to provide stability to the flat front. A linear stability analysis shows that the transition from stable to unstable flat fronts can be oscillatory for viscous fluid motion. Once the transition takes place, the fronts exhibit oscillatory convection resulting in oscillations of the shape and speed of the front.

DOI: 10.1103/PhysRevE.98.023102

## I. INTRODUCTION

Several processes in nature involve two different substances separated by a thin moving interface. We find examples of these processes in directional solidification [1], liquid-gas interfaces [2], combustion [3,4], or reaction-diffusion fronts [5,6]. In those cases, the substances have different properties, such as temperature, viscosity, or density. The time evolution of the interface can be described with an equation that depends on the front position and its derivatives. In the case of fluid substances, hydrodynamics will affect the propagation of the front. In the presence of gravity, fluid motion will tend to destabilize a flat interface through the Rayleigh-Taylor (RT) instability [7]. This instability mechanism takes place if a fluid of higher density is placed above a lower density fluid. In the reverse situation (the less dense fluid on top), fluid motion will tend to stabilize the system. Additional mechanisms, such as the presence of surface tension, may have an impact on the front stability [8]. Depending on the particular physical system, a flat front can become unstable to infinitesimal perturbations through other mechanisms. One such mechanism for front instability is the diffusive instability in reaction-diffusion fronts, which is caused by chemicals of different diffusivities [9,10] or different diffusional fluxes due to the production of the autocatalyst [11–13]. These types of fronts can be also be described using a Kuramoto-Sivashinsky (KS) equation which exhibits a flat front instability for perturbations of large wavelengths [14,15]. Previous works have studied the interaction of diffusive instabilities with the RT instability by coupling hydrodynamics to a reaction-diffusion system of equations [16,17]. Other works look at the effects of the RT instability on potentially unstable fronts described by the KS equation [18,19]. In both cases, the hydrodynamics was described by Darcy's law applied to fluids confined in Hele-Shaw cells or in porous media. It was found that favorable buoyancy forces contribute to the flat front instability, whereas, in the reverse situation, they help stabilize a mechanism that destabilizes the front. The transition to convection was found to be stationary, where the growth rate for small perturbations has zero real and imaginary parts.

In this work, we look for oscillatory flat front instabilities due to the presence of density gradients across the front. We use the KS equation to describe the motion of a moving front coupled with the Navier-Stokes equations to account for the motion of the viscous fluid. We will show that an oscillatory instability can exist depending on the value of a Schmidt number that is proportional to the fluid viscosity. Although the instability found using the KS equation alone is stationary, an adverse density gradient not only can provide stability to the front, but it can also generate an oscillatory transition where the growth rate for small perturbations has a zero real part, but a nonzero imaginary part. We also carry out a numerical solution of the nonlinear system of equations showing the presence of fronts that exhibit oscillations in shape and speed.

## II. EQUATIONS OF MOTION

We study thin reaction fronts that separate reacted from unreacted fluids in a viscous media. The front can be described with a height function $H(X,T)$ that provides the vertical position of the front as a function of the horizontal coordinate $X$ and the time $T$. In this work we focus on fronts that obey the KS equation coupled with fluid motion

$$\frac{\partial H}{\partial T} = V_0 + \mathcal{V}\frac{\partial^2 H}{\partial X^2} + \frac{V_0}{2}\left(\frac{\partial H}{\partial X}\right)^2 - \mathcal{K}\frac{\partial^4 H}{\partial X^4} + V_z|_H. \quad (1)$$

The coefficients $\mathcal{V}$ and $\mathcal{K}$ determine the evolution of the front without fluid motion and depend on the parameters of the system under consideration. For fronts that exhibit diffusive instabilities, the coefficient $\mathcal{V}$ depends on the ratio of the diffusivities of the different chemical substances involved [9,15]. It can be either positive or negative, which determines the stability of flat front solutions without fluid motion ($V_z = 0$). If $\mathcal{V} > 0$, the flat front solution of Eq. (1) is stable to perturbations of all wavelengths, but when $\mathcal{V} < 0$, this solution

 

becomes unstable to large wavelength perturbations. In the particular case of a cubic autocatalytic reaction where both diffusivities are the same, the coefficients become $\mathcal{K} = 0$ and $\mathcal{V} = D$, where $D$ is the molecular diffusivity [15]. In other systems, such as the case of thermodiffusive instabilities, they will depend on the corresponding thermal diffusion coefficient [14,20]. The equation involves the flat front speed $V_0$ and the vertical component of the fluid velocity $V_z$, which is evaluated at the front height $H$. Since we are studying fronts near the onset of convection, we assumed that the fluid velocity is small, providing a term comparable to a second order correction on the front height [18,21].

In this paper, we use a two-dimensional Navier-Stokes equation to describe viscous fluid motion

$$\frac{\partial \vec{V}}{\partial T} + (\vec{V}\cdot\nabla)\vec{V} = -\frac{1}{\rho_0}\nabla P + \nu\nabla^2\vec{V} - \frac{\rho}{\rho_0}g\hat{z}. \tag{2}$$

The velocity field must satisfy the continuity equation

$$\vec{\nabla}\cdot\vec{V} = 0. \tag{3}$$

Here $\vec{V}$ is the fluid velocity, $P$ is the pressure, $g$ is the acceleration of gravity, $\hat{z}$ is a unit vector in the vertical $Z$-direction pointing upward, $\nu$ is the coefficient of kinematic viscosity, $\rho_0$ is the density of the unreacted fluid, and $\rho$ corresponds to the fluid density that depends on the chemical composition. In the thin front approximation, there is an abrupt change of density across the front that can be written as

$$\rho = \rho_0 + \Delta\rho\Theta(Z - H), \tag{4}$$

where $\Theta$ is the a step function, being equal to one if the argument is positive and zero otherwise. The density difference between unreacted and reacted fluid corresponds to $\Delta\rho$, being positive if the heavier fluid is on top. The continuity equation allows us to write the components of the fluid velocity in terms of a stream function $\Psi(X, Z, T)$, using $V_x = \partial\Psi/\partial Z$ and $V_z = -\partial\Psi/\partial X$. Introducing these relations into the Navier-Stokes equations [Eq. (2)] and combining them to eliminate the pressure, we obtain the following equation for the stream function $\Psi$ and the vorticity $\Omega$:

$$\frac{\partial\Omega}{\partial t} = \frac{\partial(\Psi,\Omega)}{\partial(X,Z)} + \nu\nabla^2\Omega + \frac{g}{\rho_0}\frac{\partial\rho}{\partial X}. \tag{5}$$

Here the vorticity is defined as

$$\Omega = \nabla^2\Psi, \tag{6}$$

while $\partial(F_1, F_2)/\partial(X, Z)$ is defined by

$$\frac{\partial(F_1,F_2)}{\partial(X,Z)} = \frac{\partial F_1}{\partial X}\frac{\partial F_2}{\partial Z} - \frac{\partial F_1}{\partial Z}\frac{\partial F_2}{\partial X}. \tag{7}$$

We use dimensionless units to write the equations of motion. Assuming that $\mathcal{K}$ is nonzero, we introduce time and length scales defined by $L_T = \mathcal{K}/\mathcal{V}^2$, and $L_x = \sqrt{(\mathcal{K}/|\mathcal{V}|)}$. We define $|\mathcal{V}|/L_x^2$ as unit of the vorticity and $|\mathcal{V}|$ as unit of the stream function. In this system of units (represented with lower case letters), the dynamic equations become

$$\frac{\partial\omega}{\partial t} = \frac{\partial(\psi,\omega)}{\partial(x,z)} + \mathrm{Sc}\nabla^2\omega - \mathrm{RaSc}\frac{\partial h}{\partial x}\delta(z-h). \tag{8}$$

These units lead to a dimensionless Rayleigh number

$$\mathrm{Ra} = \frac{g\delta\rho L^3}{\nu|\mathcal{V}|}. \tag{9}$$

Here $\delta\rho$ corresponds to the fractional density difference between the unreacted and reacted fluid, and Sc is a dimensionless Schmidt number defined as

$$\mathrm{Sc} = \frac{\nu}{|\mathcal{V}|} \tag{10}$$

since the parameter $\mathcal{V}$ corresponds to the molecular diffusivity in cubic autocatalytic reaction fronts with a single diffusive substance.

In these units, the KS equation (1) becomes

$$\frac{\partial h}{\partial t} = c_0 - \frac{\partial^2 h}{\partial x^2} + \frac{c_0}{2}\left(\frac{\partial h}{\partial x}\right)^2 - \frac{\partial^4 h}{\partial x^4} - \left.\frac{\partial\psi}{\partial x}\right|_h, \tag{11}$$

which involves a dimensionless front speed $c_0$ using the corresponding time and length scales ($c_0 = V_0 L_T/L_x$). As discussed earlier, we consider only the case of negative coefficient $\mathcal{V}$, when the KS equation has a long wavelength instability in the absence of fluid motion [14]. Equations (8)–(11) allow a flat front solution $h_0(x, t) = 0$ with stream function $\psi_0(x, z, t) = c_0 x$, in a reference frame moving with the flat front velocity $c_0$. We define a stream function $\psi'$, relative to the stream function $\psi_0$, using the relation $\psi = \psi' + \psi_0$. Therefore our equations in the moving frame read as

$$\frac{\partial\omega}{\partial t} = c_0\frac{\partial\omega}{\partial z} + \frac{\partial(\psi',\omega)}{\partial(x,z)} + \mathrm{Sc}\nabla^2\omega - \mathrm{RaSc}\frac{\partial h}{\partial x}\delta(z-h) \tag{12}$$

and

$$\frac{\partial h}{\partial t} = -\frac{\partial^2 h}{\partial x^2} + \frac{c_0}{2}\left(\frac{\partial h}{\partial x}\right)^2 - \frac{\partial^4 h}{\partial x^4} - \left.\frac{\partial\psi_1}{\partial x}\right|_h. \tag{13}$$

### A. Linear stability analysis

We carry out a linear stability analysis of the flat front solution neglecting the nonlinear terms in Eqs. (12) and (13), given that the zeroth-order solution corresponds to zero front height and zero stream function. We introduce perturbations of the form

$$\psi' = \hat{\psi}(z)e^{\sigma t}\sin(qx) \tag{14}$$

and

$$h = h_1 e^{\sigma t}\cos(qx) \tag{15}$$

into the linearized equations, leading to

$$\sigma\left(\frac{d^2}{dz^2} - q^2\right)\hat{\psi} = c_0\left(\frac{d^2}{dz^2} - q^2\right)\frac{d\hat{\psi}}{dz} - \mathrm{Sc}\left(\frac{d^2}{dz^2} - q^2\right)^2\hat{\psi} + \mathrm{RaSc}qh_1\delta(z) \tag{16}$$

and

$$\sigma h_1 = (q^2 - q^4)h_1 - q\hat{\psi}(0). \tag{17}$$

The strategy for solving this system consists in first solving the linear equation (16) in terms of $h_1$ and then substituting into Eq. (17). The delta function leads to the following jump

conditions at $z = 0$:

$$[\hat{\psi}] = \left[\frac{d\hat{\psi}}{dz}\right] = \left[\frac{d^2\hat{\psi}}{dz^2}\right] = 0 \quad \text{and} \quad \left[\frac{d^3\hat{\psi}}{dz^3}\right] = -\mathrm{Ra}qh_1. \tag{18}$$

Here the brackets represent the value of the function just above the front minus the value of the function just below the front. We look for solutions of the homogeneous part of Eq. (16) substituting $\hat{\psi} = \psi_k e^{kz}$. This leads to an equation in the wave number $k$:

$$(k^2 - q^2)\left(k^2 + \frac{c_0}{\mathrm{Sc}}k - q^2 - \frac{\sigma}{\mathrm{Sc}}\right) = 0. \tag{19}$$

From here we obtain four values for $k$, namely $k_{1,2} = \pm q$ and $k_{3,4} = -\sigma/\mathrm{Sc} \pm q_2$, where

$$q_2 = \sqrt{\gamma_0^2 + 4(q^2 + \sigma/\mathrm{Sc})} \tag{20}$$

with $\gamma_0 = c_0/\mathrm{Sc}$. Since the solution has to be finite far away from the front, it can be written as

$$\psi_1(z) = \begin{cases} Ae^{-qz} + Be^{k_4} & \text{if } z \geqslant 0 \\ Ce^{qz} + De^{k_3} & \text{if } z < 0 \end{cases}, \tag{21}$$

where the jump conditions require that the coefficients A, B, C, and D satisfy

$$A + B - C - D = 0, \tag{22}$$

$$qA - k_4 B + qC + k_3 D = 0, \tag{23}$$

$$q^2 A + k_4^2 B - q^2 C - k_3^2 D = 0, \tag{24}$$

$$q^3 A - k_4^3 B + q^3 C + k_3^3 D = \mathrm{Ra}\, qh_1. \tag{25}$$

The solution to this system of equations leads to

$$\hat{\psi}(0) = C + D = \frac{h_1 \mathrm{Ra}}{2} \frac{(2q + k_3 - k_4)}{(-k_3 + k_4)(q + k_3)(q - k_4)}.$$

Substituting into Eq. (17) and using the definitions of $k_3$ and $k_4$ we arrive at the equation

$$2q_2(\sigma - q^2 + q^4)\left[(q + q_2)^2 - \gamma_0^2\right] = \mathrm{Ra}\, q(q + q_2). \tag{26}$$

This equation represents the dispersion relation between the growth rate $\sigma$ and the wave number $q$. It depends on three parameters: the Rayleigh number Ra, the Schmidt number Sc, and the dimensionless parameter $\gamma_0$.

### B. Numerical solutions

We look for numerical solutions of the nonlinear equations in the weakly nonlinear regime, keeping only linear terms in the the vorticity and stream function, assuming that we are close to a flat front instability. We also consider that the front deviates only slightly from the flat front, therefore we evaluate the delta function at the average front position, instead of the local front position. With these simplifications, we introduce Fourier series expansions in the horizontal $x$ direction:

$$\psi = \sum_{n=1} \psi_n(z, t) \sin(nqx), \tag{27}$$

$$\omega = \sum_{n=1} \omega_n(z, t) \sin(nqx), \tag{28}$$

and

$$h = \sum_{n=0} H_n(t) \cos(nqx). \tag{29}$$

Here the parameter $q$ is corresponds to $q = \pi/a$, where $a$ is the width of the domain. Each Fourier series corresponds to the appropriate boundary conditions at the vertical walls: horizontal fluid velocity zero ($v_x = 0$) and zero first and third derivatives for the front height ($\partial h/\partial x = \partial h^3/\partial x^3 = 0$) [22]. We assume slip-free boundary conditions. Substituting into the equations of motion and projecting over the corresponding sine and cosine functions, we obtain

$$\frac{\partial \omega_n}{\partial t} = \mathrm{Sc}\left[\frac{\partial^2 \omega_n}{\partial z^2} - (nq)^2 \omega_n\right] + \mathrm{RaSc}\delta(z - H_0), \tag{30}$$

$$\frac{\partial^2 \psi_n}{\partial z^2} - (nq)^2 \psi_n = \omega_n, \tag{31}$$

$$\frac{dH_0}{dt} = c_0 + \frac{q^2}{4} \sum_p p^2 H_p^2, \tag{32}$$

$$\frac{dH_n}{dt} = \left[(nq)^2 - (nq)^4 + \mathrm{Ra}\frac{nq}{2}\right] H_n - nq\psi_n(H_0, t) + \frac{q^2}{4} c_0 \sum_{l,p} lpH_p H_l(\delta_{n,|l-p|} - \delta_{n,l+p}),$$

$$\text{for } n \geqslant 1. \tag{33}$$

We solve these equations numerically using central finite differences to discretize the spatial derivatives on a spatial mesh made of 500 points having a grid size $\Delta z = 0.04$. The time evolution is carried out using a Runge-Kutta method of order 2, with a constant time step $\Delta t = 0.0012$. This requires one to calculate the variables $\omega_n$ at a half-time step and later at the full time step. With these values of $\omega_n$, we obtain $\psi_n$ from Eq. (31) using a tridiagonal matrix solver. We use the value of $\psi_n$ at the average front position $H_0$ to advance the front expansion coefficients $H_n$.

## III. RESULTS

We obtain the dispersion relation between the growth rate $\sigma$ and the wave number $q$ by solving Eq. (26). The values of the real part of the growth rate will determine the stability of the flat front. We first focus on the solutions where the Schmidt number is $\mathrm{Sc} = 0.588$ and the parameter $\gamma_0 = 0$. We chose these values since they illustrate direct transitions to convection. When the front is not coupled to fluid motion ($\mathrm{Ra} = 0$), the growth rate is a real number (no imaginary part). In this situation the growth rates have positive values for $q < 1$ indicating long wave instabilities [19]. Increasing the Rayleigh number to positive values increases the range of wave numbers that allow unstable fronts, thus the front is easier to destabilize. This is a consequence of buoyancy forces, since a positive Rayleigh number arises from having a lighter fluid underneath a heavier fluid. On the other hand, having the lighter fluid on top (negative Rayleigh numbers) should provide stability to the initially unstable front. From Eq. (26) we obtain multiple solutions for the growth rate for a given value of $q$. The stability of these perturbations is determined by the real parts of the growth rates: if the largest value is negative, then

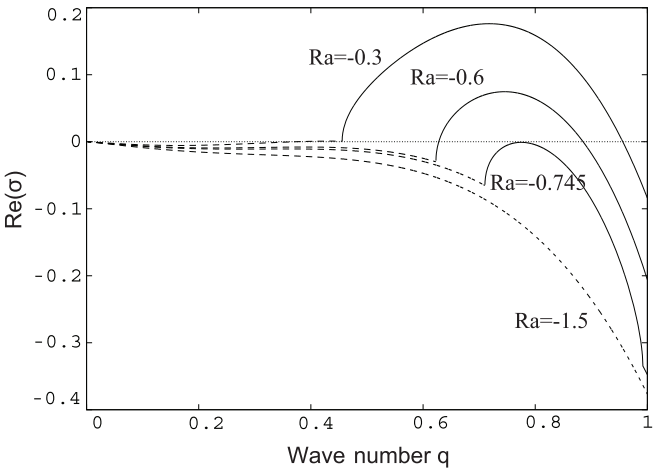


FIG. 1. The largest value of $\mathrm{Re}(\sigma)$ as a function of the wave number for $\mathrm{Sc} = 0.588$. Dashed lines indicate growth rates with nonzero imaginary part. Solid lines correspond to purely real growth rates.

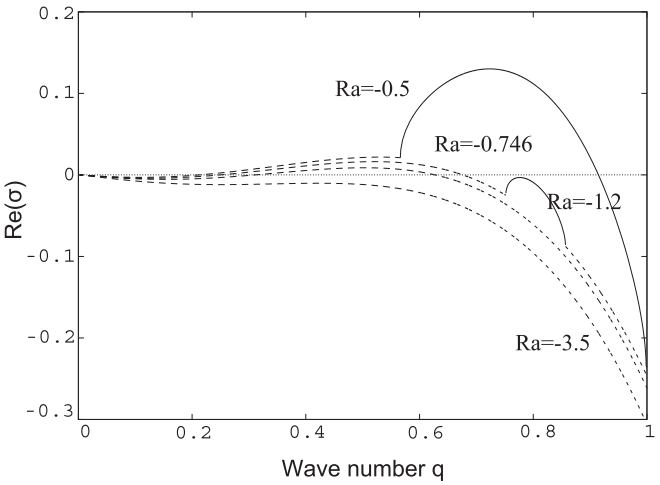


FIG. 2. The largest value of $\mathrm{Re}(\sigma)$ as a function of the wave number for $\mathrm{Sc} = 0.4$. Dashed lines indicate growth rates with nonzero imaginary part. Solid lines correspond to purely real growth rates.

the flat front is stable. Since positive Rayleigh numbers always increase the instability of the already unstable flat front in the KS equation, we focus only on negative Rayleigh numbers. As we decrease the Rayleigh number from $\mathrm{Ra} = -0.03$ to $\mathrm{Ra} = -0.6$, the range of wave numbers that lead to unstable perturbations [that is, wave numbers with $\mathrm{Re}(\sigma)$ positive] decreases (Fig. 1). Decreasing it even further to $\mathrm{Ra} = -1.5$ results in a stable flat front for all perturbations, regardless of the wave number $q$. We find that the critical value of the Rayleigh number that separates stable from unstable flat fronts corresponds to $\mathrm{Ra} = -0.745$. For cases where $\mathrm{Ra} \geqslant -0.745$, the curves show a positive relative maximum that increases with increasing Rayleigh number. They also show a slope discontinuity that disappears when the Rayleigh number takes large negative values such as $\mathrm{Ra} = -1.5$. The slope changes abruptly because we display only the largest value of $\mathrm{Re}(\sigma)$, with the other solutions not shown. If they were shown, they would be smooth curves crossing each other. We point out that the growth rates near $q = 0$ have a nonzero imaginary part, becoming purely real numbers once the wave number $q$ reaches the slope discontinuity. The curve with $\mathrm{Ra} = -0.3$ is the only one that allows unstable perturbations with nonzero imaginary part, while for all other curves in Fig. 1 the complex growth rates have negative real parts. The transition from stable to unstable flat fronts that takes place at $\mathrm{Ra} = -0.745$ corresponds to a stationary transition since the growth rate with the largest $\mathrm{Re}(\sigma)$ has a corresponding imaginary part equal to zero.

The transition from stable to unstable fronts becomes oscillatory when we set the Schmidt number to $\mathrm{Sc} = 0.4$ and increase the Rayleigh number. With this Schmidt number, the front is stable for $\mathrm{Ra} = -3.5$ having the real part of the growth rate $\mathrm{Re}(\sigma)$ negative for all wave numbers as shown in Fig. 2. Increasing the Rayleigh number to $\mathrm{Ra} = -1.2$ results in a range of positive values for $\mathrm{Re}(\sigma)$, all the corresponding growth rates have a nonzero imaginary part, signaling an oscillatory instability. The transition to this oscillatory regime occurs at $\mathrm{Ra} = -2.0$. For larger values of Ra, each curve displays discontinuities in the slope similar to the ones shown in Fig. 1, due to the crossover between multiple solutions for $\sigma$ [recall that we plot only the largest $\mathrm{Re}(\sigma)$]. Here we observe the formation of a new relative maximum for $\mathrm{Re}(\sigma)$ that has a corresponding imaginary part equal to zero. This maximum value becomes positive at $\mathrm{Ra} = -0.746$, which is slightly different from the critical value for the transition to unstable fronts in the previous case ($\mathrm{Sc} = 0.588$), but here the front is already unstable since there is a range of wave numbers $q$ corresponding to destabilizing perturbations. The fastest growing mode corresponds to an oscillatory mode. Increasing the Rayleigh number further to $-0.5$ results in having both stationary and oscillatory destabilizing perturbations taking place at different wave number, with the fastest growth rate corresponding to a direct, nonoscillatory mode. Changing the Schmidt number from $\mathrm{Sc} = 0.588$ to $\mathrm{Sc} = 0.4$ results in changing the type of instability: from a a direct to an oscillatory instability.

The critical values of the Rayleigh number for the change from stable to unstable fronts vary with respect to the Schmidt number. Moreover, the Schmidt number will determine whether the transition is stationary or oscillatory. The critical Rayleigh number is determined when the absolute maximum of $\mathrm{Re}(\sigma)$ is equal to zero. We found that the dispersion curves can have either one or two relative maximums for $\mathrm{Re}(\sigma)$ as a function of the wave number, as shown in Fig. 1 and Fig. 2, depending on the Rayleigh number. When there are two maximum values, one of them has nonzero imaginary part for the growth rate, while at the other maximum, the corresponding imaginary part of the growth rate is zero. When the largest of these two maxima is equal to zero the front is at the transition to instability.

In Fig. 3 we display the Rayleigh numbers necessary to make each relative maximum for $\mathrm{Re}(\sigma)$ equal to zero, keeping the parameter $\gamma_0$ equal to zero. The transition occurs at the smallest of these Rayleigh numbers. Therefore, only the region under under both curves correspond to values of Ra and Sc that allows stable fronts. We notice that the line corresponding to stationary transitions is almost flat, although it has a slight

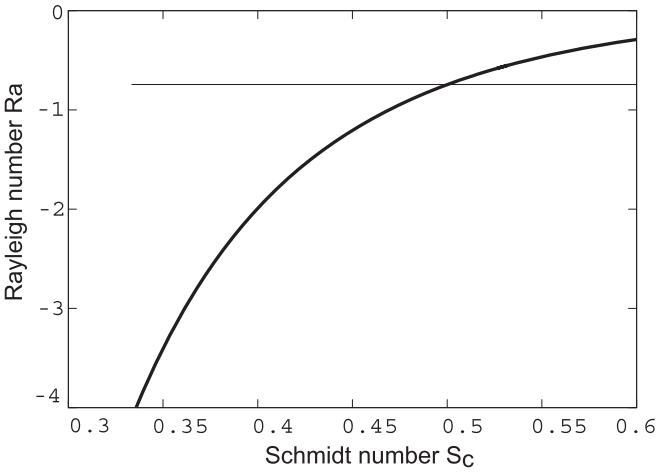


FIG. 3. Marginal stability curves for the stationary instability (thin line) and the oscillatory instability (bold line). For values of $\mathrm{Sc} < 0.5$ the oscillatory instability takes place at Rayleigh numbers lower than the stationary transition.

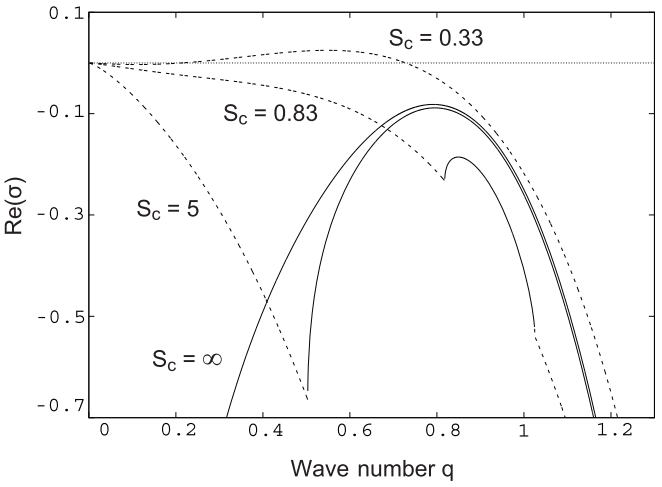


FIG. 5. Real part of the growth rate for different values of the Schmidt number Sc. Here we set $\mathrm{Ra} = -1$ and $\gamma_0 = 0$. Dashed lines indicate growth rates with nonzero imaginary part. Solid lines correspond to purely real growth rates.

dependence on Sc. We notice that the stationary transition occurs at $\mathrm{Sc} = 0.50$, and that for higher values of Sc the curve for stationary transitions is located below the curve corresponding to oscillatory transitions.

The effect of the parameter $\gamma_0$ (which is proportional to the flat front velocity) on the transition to convective fronts is displayed in Fig. 4. Here we display the critical Rayleigh number for the transition to convective fronts as a function of the Schmidt number for four different values of $\gamma_0$. Each curve consists of an increasing portion, joining an almost flat line at a certain value of Sc. The area below each curve correspond to parameters that determine stable flat fronts. For a given Schmidt number, the transition to convective fronts occurs as the Rayleigh number crosses the curve. If it crosses through the nearly flat part of the curve, the transition to convection would be direct. This occurs at all values of $\gamma_0$ for large enough Schmidt number. On the other hand,

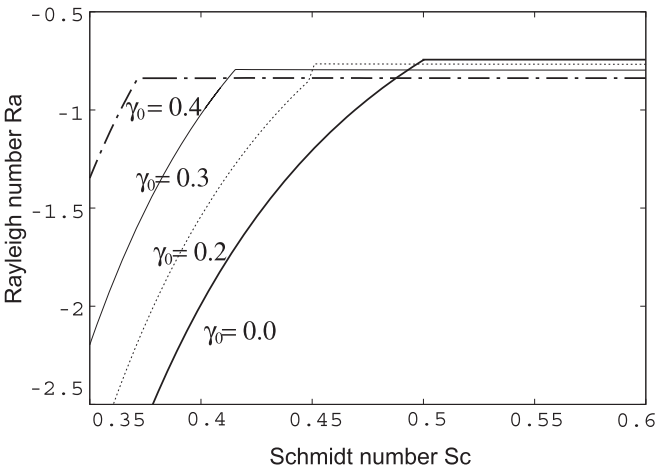


FIG. 4. Marginal stability curves for the transition to convection for different values of the parameter $\gamma_0$. The area under each curve corresponds to values of the Rayleigh and Schmidt numbers where the convectionless flat front is stable.

small values of the Schmidt number make the transition to convection oscillatory. As we increase the parameter $\gamma_0$, oscillatory convection requires smaller values of Sc. This is observed in Fig. 4 since the point of slope discontinuity takes place at smaller Sc on the curves with larger $\gamma_0$. We also notice that the critical Rayleigh number for oscillatory transition decreases with a larger value of $\gamma_0$ but increases for the stationary transition. For example, at $\mathrm{Sc} = 0.56$, both cases $\gamma_0 = 0$ and $\gamma_0 = 0.3$ have an oscillatory transition, with the critical Rayleigh numbers being equal to $-0.74$ and $-0.79$, respectively, that is, with the larger value corresponding to the smaller $\gamma_0$. But changing the Schmidt number to $\mathrm{Sc} = 0.39$, we find critical Rayleigh numbers equal to $-2.2$ and $-0.12$ respectively, which is the reversed relationship. Changing the direction of the front propagation, thus reversing the sign of $\gamma_0$, results in exactly the same values since Eq. (26) is invariant to sign change. For all the values of $\gamma_0$ studied, we find that the instability changes from oscillatory to stationary by increasing the Schmidt number.

The Schmidt number plays a crucial role in determining the dispersion relation between the growth rate $\sigma$ and the wave number $q$. It determines whether the transition to an unstable front is oscillatory or direct, as discussed above. We explore the dependence of the dispersion relation with respect to the Schmidt number in Fig. 5, where we display $\mathrm{Re}(\sigma)$ as a function of the wave number $q$, while keeping the Rayleigh number constant $\mathrm{Ra} = -1$ and the parameter $\gamma_0 = 0$. We observe that for a relatively small value of $\mathrm{Sc} = 0.33$, the dispersion relation has a range of wave numbers that correspond to unstable perturbations to the front. In this case all growth rates have a nonzero imaginary part, therefore small initial perturbations will lead to oscillatory fronts. For a somewhat larger value of $\mathrm{Sc} = 0.83$, we find that the flat front is stable for all perturbations. Here the growth rate is also a complex number with a nonzero imaginary part, except for an interval between two slope discontinuities that includes a relative maximum for the corresponding curve in Fig. 5. Increasing the Schmidt number to $\mathrm{Sc} = 5$, we find a similar

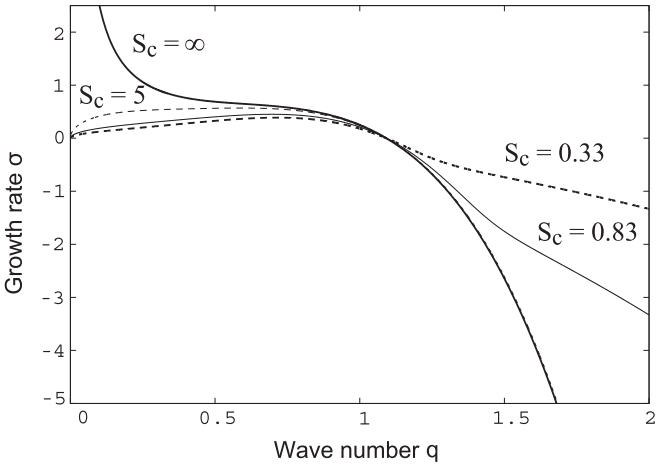


FIG. 6. Growth rates for different values of the Schmidt number Sc. Here we set Ra = 1 and $\gamma_0 = 0$.

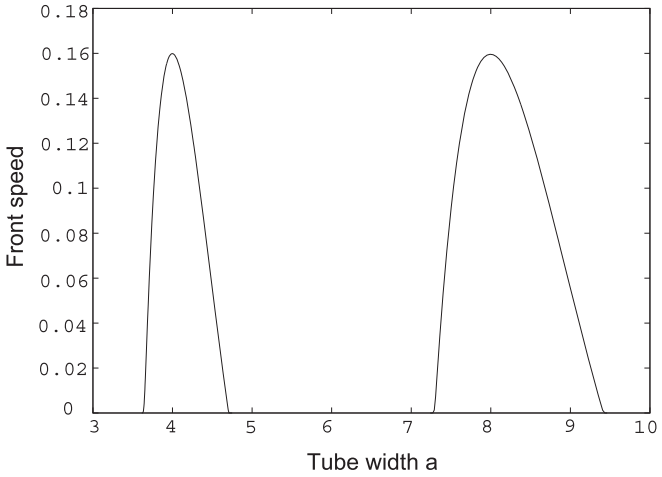


FIG. 7. The speed of steady fronts confined in a two-dimensional tube of width $a$. Here we have Ra $= -0.66$, $\gamma_0 = 0$, and Sc $= 0.588$.

situation, but now the region containing the relative maximum has grown. In the limit, when Sc $\to \infty$, we can find an analytical solution to the dispersion relation of Eq. (26):

$$\sigma = q^2 - q^4 + \mathrm{Ra}/(4q),$$

and the corresponding curve has no imaginary values for the growth rate, showing a singularity at $q = 0$. In this limiting case, there exists a single negative maximum for the growth rate, signaling stability for the flat front. Using this equation, we find that the maximum value of $\mathrm{Re}(\sigma)$ is always negative for Ra $< -0.185903$, having a critical wave number equal to $\sqrt{3/5}$.

If the Rayleigh number is positive (that is, denser fluid on top), we find that the fastest growing perturbation for a given wave number corresponds to a real number (imaginary part equal to zero), regardless of the value of the Schmidt number. In all these cases the growth rate is positive for wave numbers sufficiently close to zero, therefore the flat front will be unstable to some perturbations. In Fig. 6 we show the largest growth rates for different values of the Schmidt number for the same Rayleigh number (Ra $= 1$). We chose the same values of Sc as in Fig. 5. We found that the growth rate has a maximum value located at smaller wave numbers for increasing Sc. This shift towards smaller wave numbers is reflected in the case when the Schmidt number approaches infinity, where the dispersion relation has a positive asymptote at $q = 0$, indicating that the fastest growing perturbations correspond to large wave numbers.

As the front propagates in a vertical rectangular domain, its behavior is determined by the horizontal width ($a$) of the box. This box resembles a two-dimensional narrow tube where the front propagates upward. The linear stability analysis tells us that flat fronts are stable for perturbations of wave numbers greater than a critical wave number $q_c$, therefore they will be stable as they propagate in tubes of width smaller than $a_c = \pi/q_c$. For fronts propagating in tubes with width greater than $a_c$, we solve numerically the nonlinear equations (32) and (33). We first choose Ra $= -0.66$, $\gamma_0 = 0$, and Sc $= 0.588$, which results in real unstable growth rates for values of $q_c < 0.862$, with a corresponding value of $a_c = 3.64$. As predicted from the linear stability analysis, small random perturbations vanish if the tube width is smaller that $a_c$. However, for widths greater than $a_c$ but smaller than 4.71 we find a curved steady front moving with constant speed, having a single maximum near one side, similar to the nonaxisymmetric fronts described in Ref. [19]. We display our the results for the increase of speed as a function of the tube width in Fig. 7. As the width increases the front propagates faster, reaching a maximum value before the speed slows down, eventually reaching zero increase of velocity. For values of $a$ greater than 4.71, the front is flat again, losing stability as the width is further increased beyond $a = 7.29$, where an axisymmetric front appears. The axisymmetric front continues to increase its speed, reaching a maximum, and then finally becoming a flat front for values of $a$ greater than 9.43. We notice that the maximum speed in both types of fronts are the same. This takes place because the axisymmetric front consists of two nonaxisymmetric solutions linked at the center of the domain. This fact is also reflected in the values of the width where the flat front changes stability: the value for the axisymmetric transition is exactly half of the value required for the nonaxisymmetric transition. The increase of speed of the axisymmetric front is equal to the increase of speed of the nonaxisymmetric front in a domain with half the size of the original width.

In the case where the flat front presents an oscillatory instability, we still find stable flat fronts using small domain widths. Increasing the width beyond a critical value results in the formation of an oscillatory front. The shape of this front resembles nonaxisymmetric fronts [19] but having an oscillatory amplitude. The instantaneous speed of the average front position oscillates between a maximum and minimum value, as shown in Fig. 8. The maximum front speed increases after the transition at width $a = 5.40$ but eventually drops back after a reaching a peak value. The minimum value of the front speed is small but nonzero, reaching a highest value, and becoming the same as the flat front speed once the width is large enough. We also notice that increasing the width beyond $a = 9.29$ brings back stable flat fronts. These fronts lose stability once again to become oscillatory fronts for widths $a > 10.76$. As in the case of steady convective fronts, the

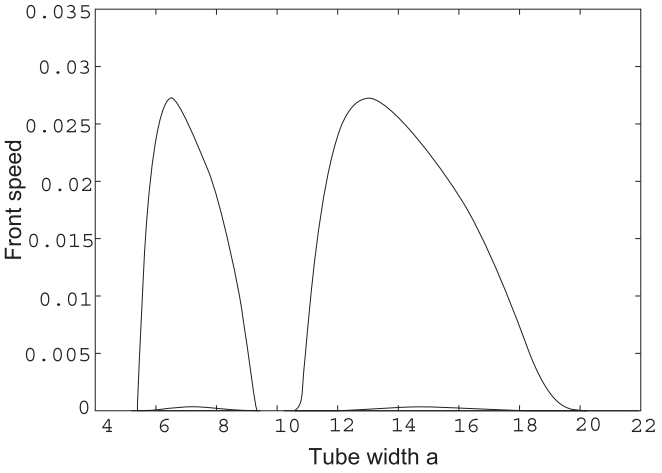


FIG. 8. The maximum and minimum speeds of the average front position as a function of tube width for oscillatory fronts. Here we have Ra $= -1.6$, $\gamma_0 = 0$, and Sc $= 0.4$.

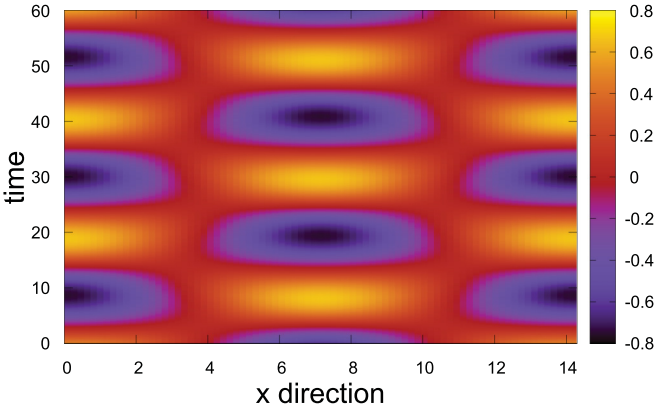


FIG. 10. Time evolution of an oscillatory front. The color map indicates the front deviation relative to the average front position. In this case, the oscillatory front is symmetric relative to the center of the tube, with its center oscillating between a maximum and minimum values.

new oscillations correspond to two nonaxisymmetric fronts, joined at the domain center, forming an axisymmetric front. The speeds of the axisymmetric fronts as functions of the width $a$ are the same as the speeds of the corresponding nonaxisymmetric fronts formed in half the domain width.

The evolution of oscillatory fronts propagating in two-dimensional tubes depends on the width of the tube. In the case of a very narrow tube only a steady flat front can propagate. Increasing the tube width beyond a critical value results in an oscillatory front for appropriate values of Ra and Sc. In Fig. 9 we display the changing shape of an oscillatory front in a tube of width $a = 6.28$. This width is just above the critical width ($a_c = 5.40$) for instability corresponding to the values of Ra $= -1.6$, and Sc $= 0.4$. In this figure we display the local front height measured with respect to the average front position. Under these conditions the front oscillates raising one side of the front while lowering the opposite side. The higher side continues to increase until its value reaches a maximum, then this height lowers to a minimum, with the inverse behavior taking place at the other side. As we increase the front width

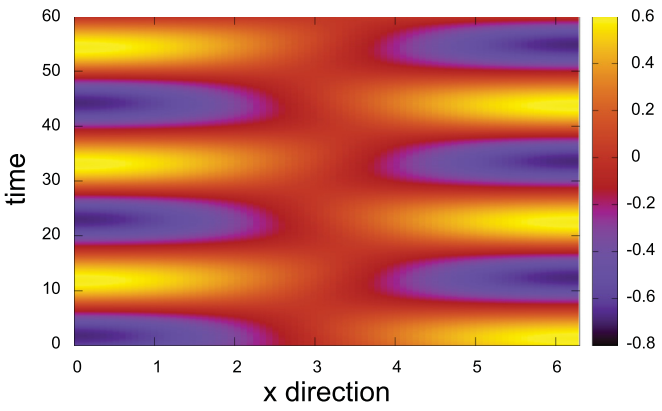


FIG. 9. Time evolution of an oscillatory front. The color map indicates the front deviation relative to the average front position. In this case, the oscillatory front has a maximum on one side of the tube, changing into a minimum as the front oscillates.

slightly above $a = 9.29$, we find that the oscillations disappear, as discussed in the previous paragraph. Then, as $a$ increases to $a = 14.2$ and above, we find an oscillatory front once again but of different shape (Fig. 10). At a particular moment, the front has a relative maximum located in the center of the domain, but as time evolves, the relative maximum becomes a relative minimum, alternating values periodically. The front is symmetric with respect to the center of the tube. On the sides of the tube, the front height opposes the central maximum (minimum) by taking its minimum (maximum) value.

## IV. SUMMARY AND DISCUSSION

We found an oscillatory transition to convection in fronts separating fluids with the lighter fluid on top. Without fluid motion, the front shows direct instabilities for perturbations of large wavelengths, with zero growth rate (real and imaginary parts) at the transition to instability. Taking into account fluid motion, density gradients can help stabilize a flat front. Nevertheless this stabilization requires a finite density difference between the substances, as reflected by the critical Rayleigh number for front stability. The interaction between the front instability and the stabilizing buoyancy force can lead to a transition to oscillatory behavior. At criticality, the growth rate of the perturbations can have a nonzero imaginary part, signaling a transition to oscillatory convection. However, depending on the Schmidt number, the transition can also be stationary. In the limiting case of an infinite Schmidt number the transition has a growth rate with zero imaginary part. Only when the Schmidt number is set below a certain value, we find the oscillatory transitions. Experiments in autocatalytic reaction fronts took place in aqueous solutions, where the Schmidt number is large. Oscillatory transitions can take place if the propagating medium is a low viscosity fluid.

The front instability is reflected in nonlinear calculations set in small rectangular domains. If the width of the domain is narrow, flat fronts are stable, since only perturbations of small wavelength are permitted inside a narrow tube. In the

case of the stationary transition, a front of constant shape and higher speed appears for widths beyond a critical value. However, increasing it further results in the disappearance of the convective front going back to a stable flat front. For even larger widths, a new stationary, steady, axisymmetric front appears. This behavior is once again observed when the flat front has an oscillatory instability for an appropriate Schmidt number. As the width of the domain is increased, an oscillatory front appears. Increasing it further allows a stable flat front once again, with a new axisymmetric oscillatory front developing for larger width values.

## ACKNOWLEDGMENT

This work was supported by a grant from the Dirección de Gestión de la Investigación (DGI 2016-3-0025) of the Pontificia Universidad Católica del Perú.

[1] J. S. Langer, Rev. Mod. Phys. **52**, 1 (1980).
[2] G. H. Wolf, Phys. Rev. Lett. **24**, 444 (1970).
[3] N. Vladimirova and R. Rosner, Phys Rev. E **67**, 066305 (2003).
[4] Z. Rakib and G. I. Sivashinsky, Combust. Sci. Tech. **54**, 69 (1987).
[5] G. Schuszter, T. Tóth, D. Horváth, and A. Tóth, Phys. Rev. E **79**, 016216 (2009).
[6] J. Masere, D. A. Vasquez, B. F. Edwards, J. W. Wilder, and K. Showalter, J. Phys. Chem. **98**, 6505 (1994).
[7] D. H. Sharp, Physica D **12**, 3 (1984).
[8] S. Chandrasekhar, *Hydrodynamic and Hydromagnetic Stability* (Oxford University Press, Oxford, 1961).
[9] D. Horváth, V. Petrov, S. K. Scott, and K. Showalter, J. Chem. Phys. **98**, 6332 (1993).
[10] D. Horváth and K. Showalter, J. Chem. Phys. **102**, 2471 (1993).
[11] É. Jakab, D. Horváth, J. H. Merkin, Á. Tóth, and S. K. Scott, Chem. Phys. Lett. **342**, 317 (2001).
[12] É. Jakab, D. Horváth, J. H. Merkin, S. K. Scott, P. L. Simon, and Á. Tóth, Phys. Rev. E **68**, 036210 (2003).
[13] D. Horváth and Á. Tóth, J. Chem. Phys. **108**, 1447 (1998).
[14] G. I. Sivashinsky, Acta Astronaut. **4**, 1177 (1977).
[15] A. Malevanets, A. Careta, and R. Kapral, Phys. Rev. E **52**, 4724 (1995).
[16] J. D'Hernoncourt, J. H. Merkin, and A. De Wit, J. Chem. Phys. **130**, 114502 (2009).
[17] J. D'Hernoncourt, J. H. Merkin, and A. De Wit, J. Chem. Phys. **130**, 114503 (2009).
[18] D. Elliott and D. A. Vasquez, Phys. Rev. E. **85**, 016207 (2012).
[19] P. M. Vilela and D. A. Vasquez, Chaos **24**, 023135 (2014).
[20] G. I. Sivashinsky, Ann. Rev. Fluid Mech. **15**, 179 (1983).
[21] R. S. Spangler and B. F. Edwards, J. Phys. Chem. **118**, 5911 (2003).
[22] S. B. Margolis and G. I. Sivsahinsky, SIAM J. Appl. Math. **44**, 344 (1984).